Supporting Information

Construction of high-performance circular polarization multiple resonance thermal activated delayed fluorescence materials via structural optimization of peripheral groups

Wenjing Li[1], *Qixin Lv*[1], *Chengxi Sun*[1], *Junyuan Deng*[1], *Cefeng Zhou*[1], *Yewen Zhang*[1], *Ping Li*[1]*, *and Runfeng Chen*[1, 2]*

[1] *State Key Laboratory of Organic Electronics andInformation Displays & Institute of Advanced Materials* (IAM), Nanjing University of Posts &Telecommunications, Nanjing 210023, P. R. China

[2] *School of Materials Science and Engineering, Zhejiang Sci-Tech University, Hangzhou 310018, P. R. China*

E-mails: iamrfchen@njupt.edu.cn

Contents

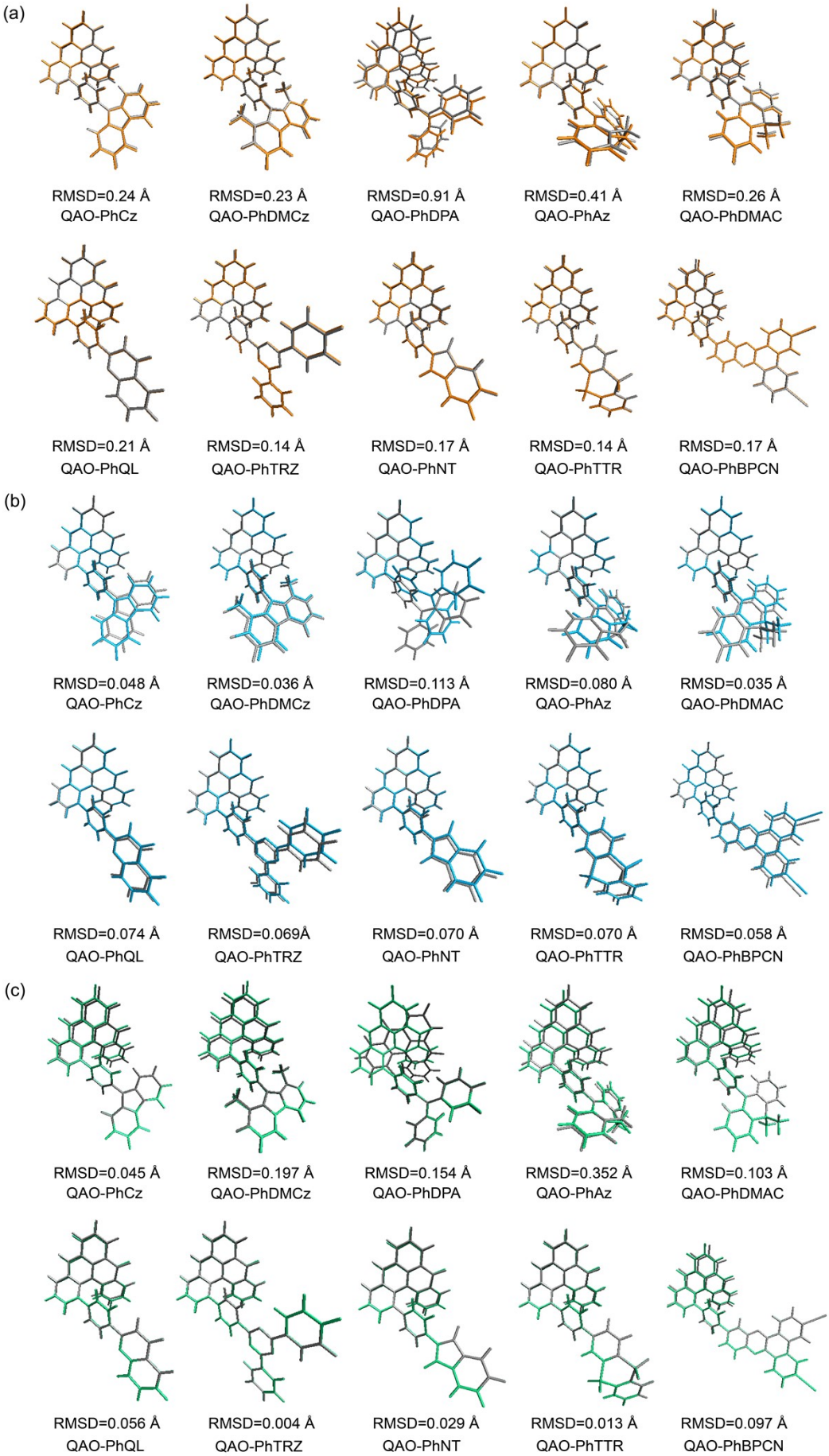
(a)
RMSD=0.24 Å
QAO-PhCz
RMSD=0.23 Å
QAO-PhDMCz
RMSD=0.91 Å
QAO-PhDPA
RMSD=0.41 Å
QAO-PhAz
RMSD=0.26 Å
QAO-PhDMAC
RMSD=0.21 Å
QAO-PhQL
RMSD=0.14 Å
QAO-PhTRZ
RMSD=0.17 Å
QAO-PhNT
RMSD=0.14 Å
QAO-PhTTR
RMSD=0.17 Å
QAO-PhBPCN
(b)
RMSD=0.048 Å
QAO-PhCz
RMSD=0.036 Å
QAO-PhDMCz
RMSD=0.113 Å
QAO-PhDPA
RMSD=0.080 Å
QAO-PhAz
RMSD=0.035 Å
QAO-PhDMAC
RMSD=0.074 Å
QAO-PhQL
RMSD=0.069Å
QAO-PhTRZ
RMSD=0.070 Å
QAO-PhNT
RMSD=0.070 Å
QAO-PhTTR
RMSD=0.058 Å
QAO-PhBPCN
(c)
RMSD=0.045 Å
QAO-PhCz
RMSD=0.197 Å
QAO-PhDMCz
RMSD=0.154 Å
QAO-PhDPA
RMSD=0.352 Å
QAO-PhAz
RMSD=0.103 Å
QAO-PhDMAC
RMSD=0.056 Å
QAO-PhQL
RMSD=0.004 Å
QAO-PhTRZ
RMSD=0.029 Å
QAO-PhNT
RMSD=0.013 Å
QAO-PhTTR
RMSD=0.097 Å
QAO-PhBPCN

Figure S1. Diagram of geometry comparisons between S_0 and S_1 states together with the calculated RMSD values for (a) the investigated molecules (the structures at S_0 and S_1 state are depicted in orange and silver, respectively), (b) the QAO part (the structures at S_0 and S_1 state are depicted in blue and silver, respectively), and (c) the phenyl-linked electron-donating/withdrawing groups (the structures at S_0 and S_1 state are depicted in green and silver, respectively).

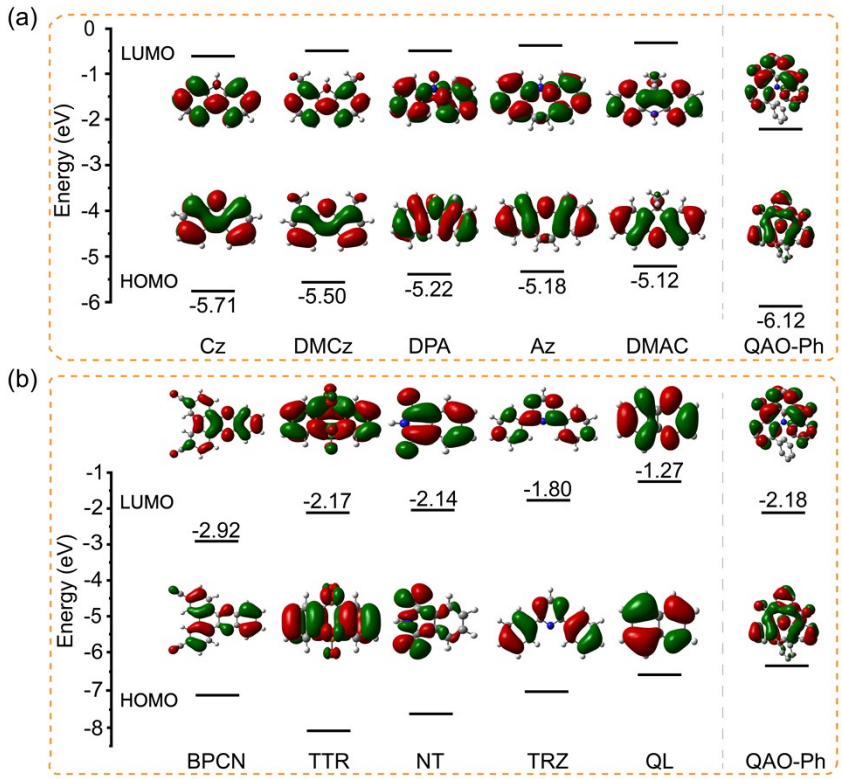

Figure S2. Calculated frontier molecular orbital (FMO) energy levels and FMO distributions of (a) the electron-donating and (b) the electron-withdrawing peripheral groups.

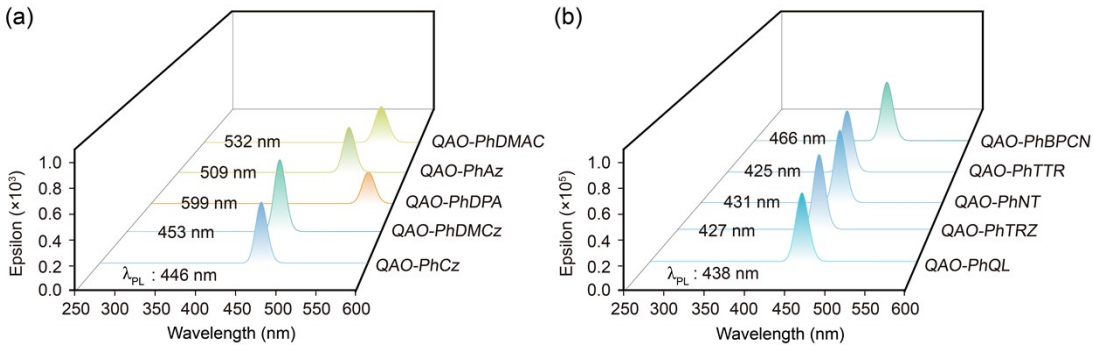

Figure S3 Simulated emission spectra of the molecules with (a) the electron-donating groups and (b) the electron-withdrawing groups (λ_{PL} in unit of nm).

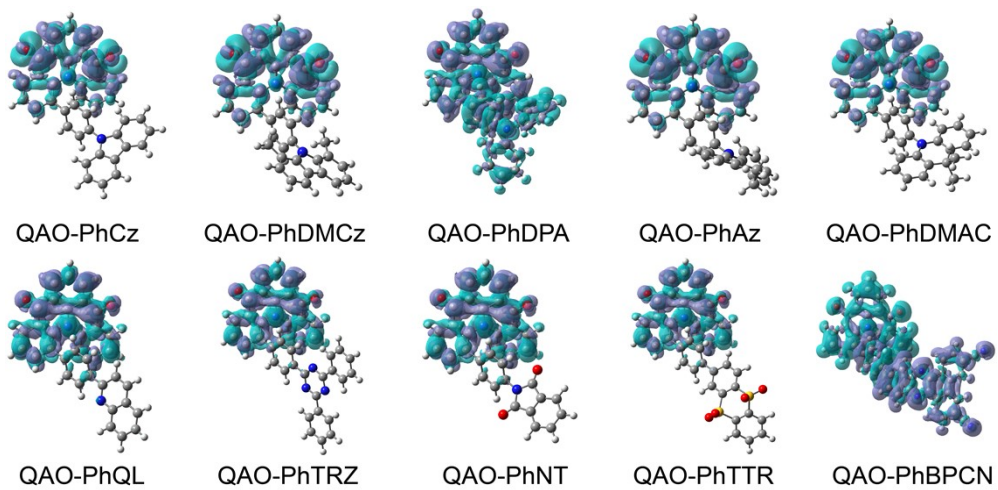

Figure S4. Charge density differences between the S_1 and S_0 of the investigated molecules.

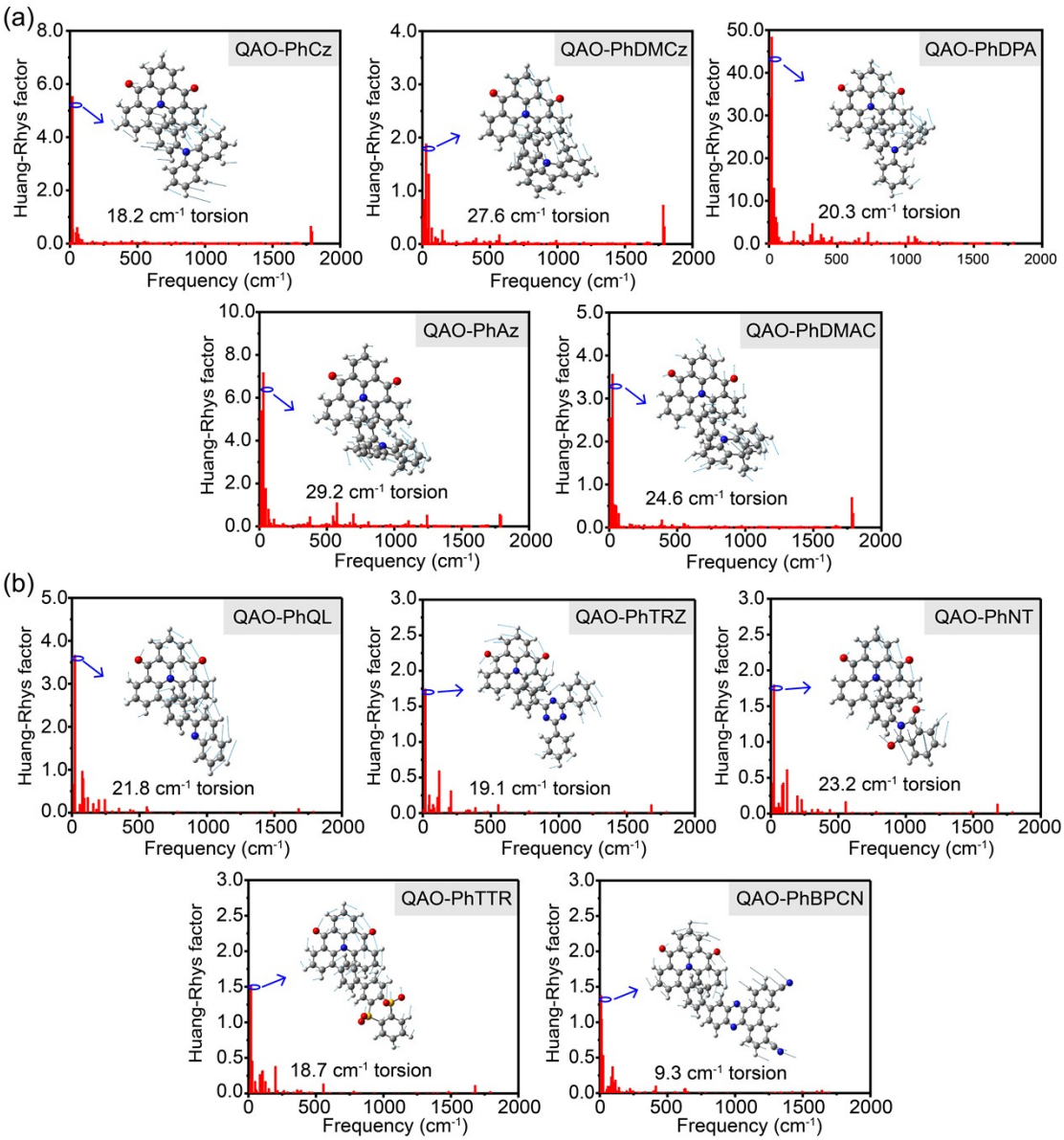

Figure S5. Calculated Huang-Rhys factors versus the normal mode frequencies for the investigated molecules with (a) the electron-donating groups and (b) the electron-withdrawing groups relevant to $S_1 \rightarrow S_0$ process (The vibration modes with relatively large Huang-Rhys factors were shown as insets).

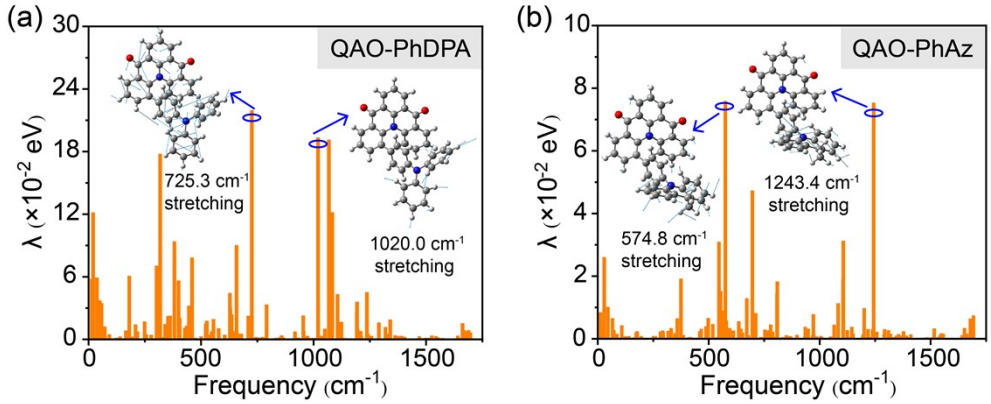

Figure S6. Calculated reorganization energies versus the normal-mode frequencies for (a) QAO-PhDPA and (b) QAO-PhAz (The representative vibration modes are shown as insets).

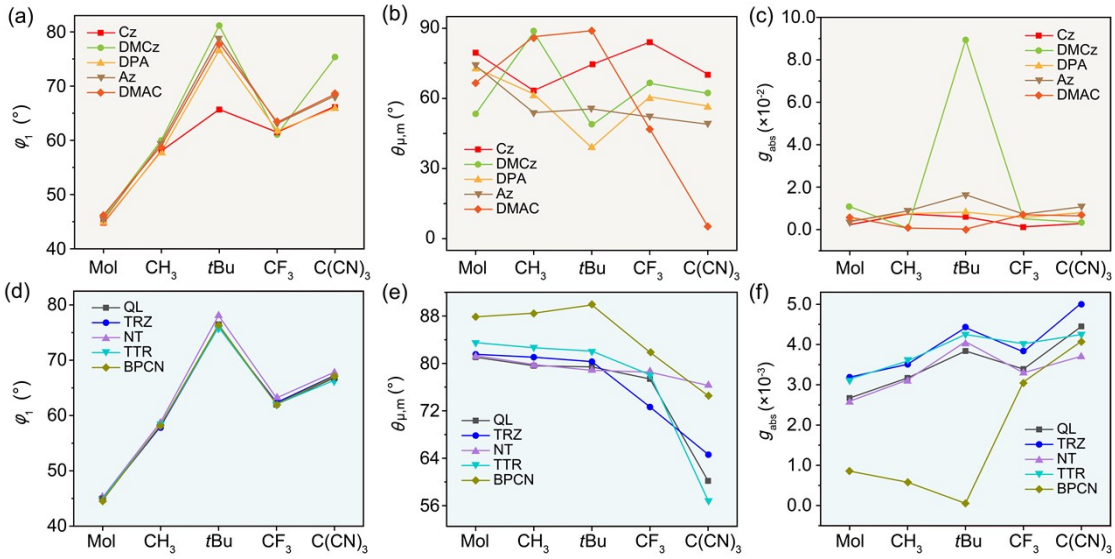

Figure S7. Calculated φ_1, $\theta_{\mu,m}$ and g_{abs} for the electron-donating- (a, b and c) and electron-withdrawing- (d, e and f) based molecules with introducing different steric hindrance groups.

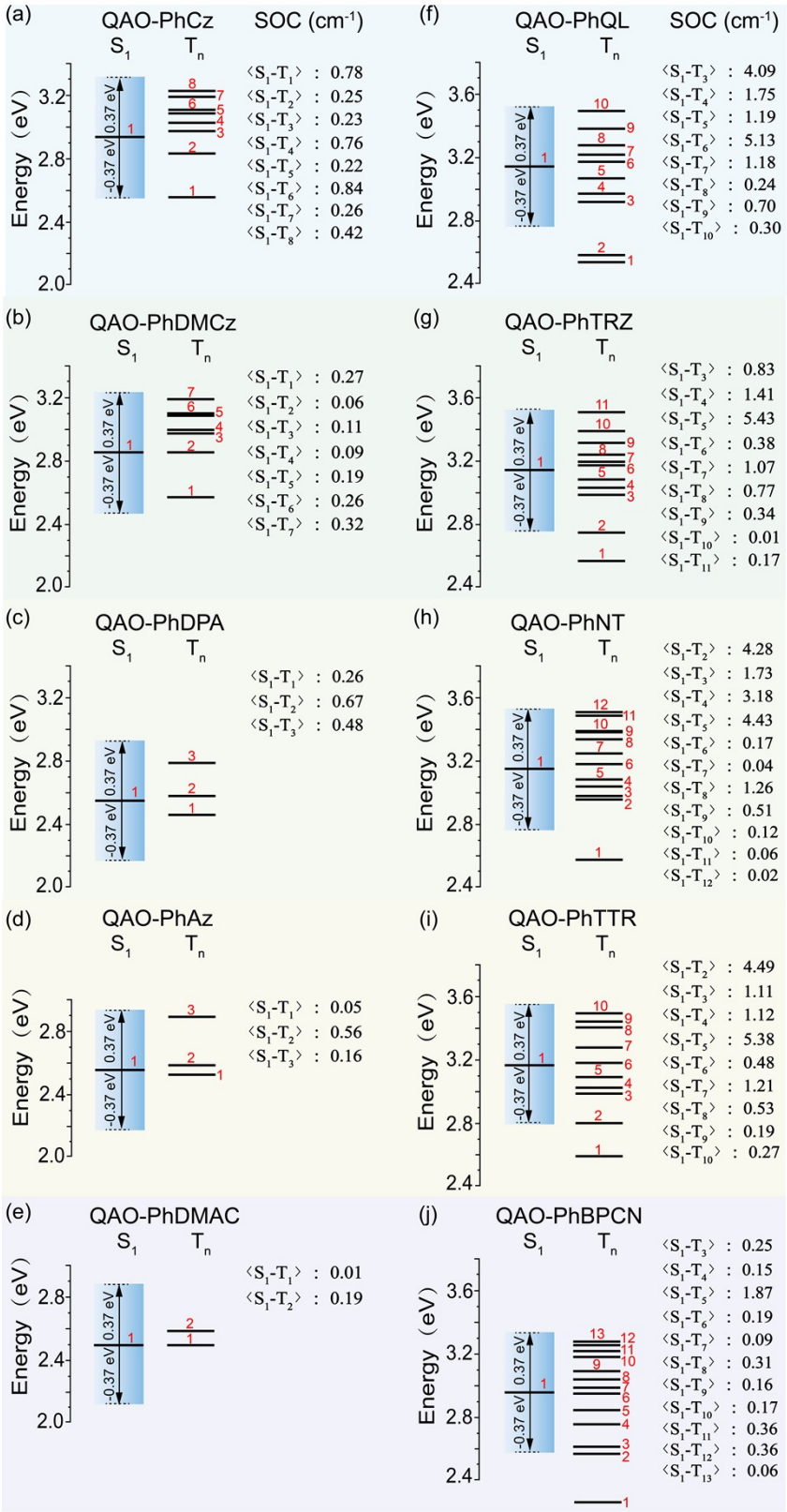

Figure S8. Calculated vertical excitation energies and the SOC constants between S_1 and T_n states for (a) QAO-PhCz, (b) QAO-PhDMCz, (c) QAO-PhDPA, (d) QAO-PhAz, (e) QAO-PhDMAC, (f) QAO-PhOL, (g) QAO-PhTRZ, (h) QAO-PhNT, (i) QAO-PhTTR and (j) QAO-PhBPCN in toluene.

Table S1. Calculated HOMO energy levels, the maximum absorption (λ_{abs}) and emission (λ_{PL}) wavelengths of the experimental molecule QAO-PhCz with different DFT functionals.

Computing method	HF (%)	HOMO (eV)	λ_{abs} / λ_{PL} (nm)
O3LYP	11.6	-5.10	525 / 622
B3LYP	20	-5.42	457 / 512
PBE0	25	-5.68	422 / 497
BMK	42	-6.13	362 / 400
M06-2X	54	-6.66	349 / 385
Exp.	--	-5.74	437 / 461

Table S2. Simulated excitation energy, transition compositions and characteristics of the molecules with electron-donating units using PBE0 and M062X functionals.

	PBE0			M062X		
	ΔE (eV)	Composition (%)	Character	ΔE (eV)	Composition (%)	Character
QAO-PhCz	2.94	H→L(97.2)	LRCT[a]	3.56	H-2→L(85.4); H-1→L(4.7); H→L(4.8)	SRCT[b]
QAO-PhDMCz	2.86	H→L(99.6)	LRCT	3.56	H-2→L(93.8)	SRCT
QAO-PhDPA	2.56	H→L(98.9)	LRCT	3.47	H→L(48.1); H-1→L(47.4)	LRCT
QAO-PhAz	2.56	H→L(99.4)	LRCT	3.55	H-1→L(88.5); H→L(6.7)	SRCT
QAO-PhDMAC	2.50	H→L(99.5)	LRCT	3.57	H-1→L(94.3)	SRCT

[a] LRCT means long-range charge transfer; [b] SRCT means short-range charge transfer

Table S3. Calculated the maximum emission wavelengths (λ_{PL}), transition compositions and reorganization energies (λ, $S_1 \rightarrow S_0$) of the investigated molecules.

Compd.	λ_{PL} (nm)	Transition compositions (%)	λ (eV)
QAO-PhCz	446	H-8→L(33.7); H-11→L(21.4);	0.32
QAO-PhDMCz	453	H-10→L(30.3); H-12→L(23.4);	0.38
QAO-PhDPA	599	H→L(92.1); H-1→L(3.5);	3.05
QAO-PhAz	509	H-8→L(29.1); H-10→L(24.9);	1.11
QAO-PhDMAC	532	H-9→L(22.8); H-12→L(22.4);	0.34
QAO-PhQL	438	H→L(95.3); H-1→L(3.0)	0.21

QAO-PhTRZ	427	H→L(98.3)	0.15
QAO-PhNT	431	H→L(98.3)	0.17
QAO-PhTTR	425	H→L(97.9)	0.15
QAO-PhBPCN	466	H→L(89.3); H-1→L(8.9)	0.15

Table S4. Calculated radiation rate (k_r, s^{-1}), nonradiative rate (k_{nr}, s^{-1}), $\theta_{\mu,m}$, g_{PL} and *FM* of the investigated molecules modified with the steric hindrance groups.

Compd.	k_r (s^{-1})	k_{nr} (s^{-1})	$\theta_{\mu,m}$ (°)	g_{PL}	*FM*
QAO-PhCz-CH_3	9.59×10^{5}	3.66×10^{7}	39.35	1.38×10^{-2}	3.53×10^{-4}
QAO-PhDMCz-CH_3	6.58×10^{5}	5.22×10^{7}	82.36	2.31×10^{-3}	2.88×10^{-5}
QAO-PhDPA-CH_3	1.26×10^{5}	3.20×10^{10}	36.86	9.94×10^{-3}	3.93×10^{-8}
QAO-PhAz-CH_3	6.69×10^{5}	1.04×10^{7}	26.21	1.81×10^{-2}	1.09×10^{-3}
QAO-PhDMAC-CH_3	4.43×10^{5}	8.82×10^{8}	18.49	3.13×10^{-2}	1.57×10^{-5}
QAO-PhQL-CH_3	2.52×10^{7}	1.15×10^{8}	76.46	3.01×10^{-3}	5.43×10^{-4}
QAO-PhTRZ-CH_3	2.58×10^{7}	3.27×10^{7}	79.36	3.25×10^{-3}	1.43×10^{-3}
QAO-PhNT-CH_3	2.87×10^{7}	2.52×10^{5}	77.19	2.91×10^{-3}	2.88×10^{-3}
QAO-PhTTR-CH_3	2.80×10^{7}	3.32×10^{7}	81.26	3.39×10^{-3}	1.55×10^{-3}
QAO-PhBPCN-CH_3	3.22×10^{6}	1.33×10^{10}	88.16	6.39×10^{-4}	1.55×10^{-7}
QAO-PhCz-*t*Bu	5.38×10^{4}	5.35×10^{9}	83.72	1.46×10^{-3}	1.47×10^{-8}
QAO-PhDMCz-*t*Bu	5.63×10^{3}	1.19×10^{9}	81.16	2.48×10^{-3}	1.17×10^{-8}
QAO-PhDPA-*t*Bu	9.47×10^{6}	2.89×10^{10}	32.71	8.34×10^{-3}	2.73×10^{-6}
QAO-PhAz-*t*Bu	8.41×10^{4}	3.09×10^{9}	17.38	1.64×10^{-2}	4.45×10^{-7}
QAO-PhDMAC-*t*Bu	6.19×10^{3}	8.24×10^{8}	28.53	1.29×10^{-2}	9.69×10^{-8}
QAO-PhQL-*t*Bu	1.68×10^{7}	7.82×10^{8}	76.70	3.71×10^{-3}	7.82×10^{-5}
QAO-PhTRZ-*t*Bu	2.04×10^{7}	2.51×10^{7}	78.05	4.37×10^{-3}	1.96×10^{-3}
QAO-PhNT-*t*Bu	1.32×10^{7}	5.38×10^{10}	75.47	4.05×10^{-3}	9.93×10^{-7}
QAO-PhTTR-*t*Bu	2.37×10^{7}	2.99×10^{5}	80.05	4.36×10^{-3}	4.31×10^{-3}
QAO-PhBPCN-*t*Bu	1.17×10^{7}	8.35×10^{9}	89.33	2.35×10^{-4}	3.30×10^{-7}
QAO-PhCz-CF_3	1.95×10^{4}	4.48×10^{10}	61.82	6.74×10^{-3}	2.95×10^{-9}
QAO-PhDMCz-CF_3	9.75×10^{6}	4.70×10^{5}	61.05	5.83×10^{-3}	5.56×10^{-3}
QAO-PhDPA-CF_3	9.84×10^{6}	4.37×10^{7}	45.85	6.05×10^{-3}	1.11×10^{-3}
QAO-PhAz-CF_3	4.68×10^{5}	2.02×10^{9}	43.38	2.49×10^{-2}	5.75×10^{-6}
QAO-PhDMAC-CF_3	2.08×10^{6}	1.75×10^{8}	23.81	1.14×10^{-2}	1.34×10^{-4}
QAO-PhQL-CF_3	8.82×10^{5}	2.90×10^{11}	54.32	8.08×10^{-3}	2.46×10^{-8}
QAO-PhTRZ-CF_3	8.11×10^{5}	7.01×10^{8}	70.52	1.11×10^{-2}	1.28×10^{-5}
QAO-PhNT-CF_3	1.27×10^{2}	6.68×10^{6}	63.25	2.89×10^{-2}	5.49×10^{-7}
QAO-PhTTR-CF_3	5.04×10^{4}	1.26×10^{11}	73.62	8.79×10^{-3}	3.51×10^{-9}
QAO-PhBPCN-CF_3	3.15×10^{4}	2.17×10^{9}	87.42	2.06×10^{-3}	3.00×10^{-8}
QAO-PhCz-$C(CN)_3$	1.03×10^{6}	1.71×10^{11}	79.03	3.49×10^{-3}	2.11×10^{-8}
QAO-PhDMCz-$C(CN)_3$	2.43×10^{3}	8.79×10^{10}	89.64	9.11×10^{-4}	2.52×10^{-11}

QAO-PhDPA-C(CN)$_3$	4.50×10^{5}	1.74×10^{11}	59.07	5.31×10^{-3}	1.38×10^{-8}
QAO-PhAz-C(CN)$_3$	1.72×10^{6}	2.90×10^{8}	42.85	6.20×10^{-2}	3.64×10^{-4}
QAO-PhDMAC-C(CN)$_3$	1.99×10^{3}	3.97×10^{10}	45.19	4.46×10^{-2}	2.23×10^{-9}
QAO-PhQL-C(CN)$_3$	6.37×10^{4}	8.81×10^{10}	78.15	4.35×10^{-3}	3.15×10^{-9}
QAO-PhTRZ-C(CN)$_3$	3.58×10^{4}	7.49×10^{10}	70.49	9.57×10^{-3}	4.57×10^{-9}
QAO-PhNT-C(CN)$_3$	6.59×10^{2}	2.43×10^{8}	53.47	2.94×10^{-2}	7.99×10^{-8}
QAO-PhTTR-C(CN)$_3$	1.44×10^{4}	5.65×10^{10}	88.07	1.13×10^{-3}	2.87×10^{-10}
QAO-PhBPCN-C(CN)$_3$	1.65×10^{4}	3.18×10^{10}	77.35	7.08×10^{-3}	3.68×10^{-9}

Table S5. Summary of the PLQY, $|g_{PL}|$ and *FM* values of the reported CP-MR-TADF materials.

Compd.	$\|g_{PL}\|$	PLQY	*FM*	Year	Reference
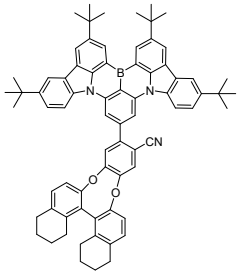 OBN-2CN-BN	9.1×10^{-4}	99%	9.0×10^{-4}	2021	1
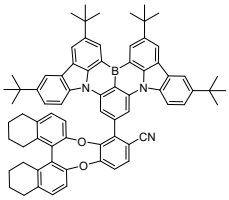 OBN-4CN-BN	10.4×10^{-4}	95%	9.9×10^{-4}	2021	
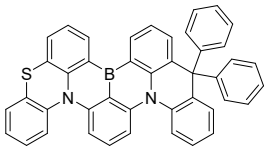 BN-4	1.0×10^{-3}	88%	8.8×10^{-4}	2021	2
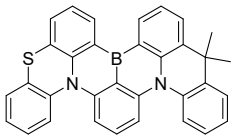 BN-5	1.0×10^{-3}	87%	8.7×10^{-4}	2021	

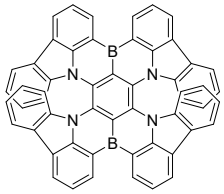 1a	2.0×10^{-3}	100%	2.0×10^{-3}	2021	
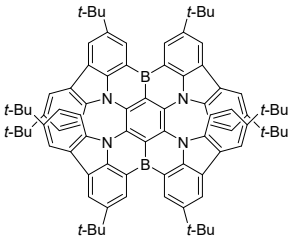 1b	2.0×10^{-3}	99%	2.0×10^{-3}	2021	3
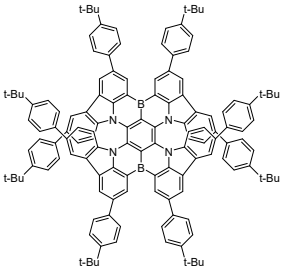 1c	2.0×10^{-3}	90%	1.8×10^{-3}	2021	
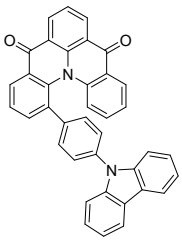 QAO-PhCz	1.1×10^{-3}	47%	5.2×10^{-4}	2021	4
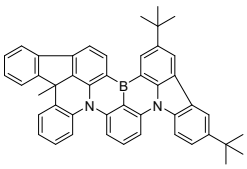 BN-MelAC	3.2×10^{-4}	96%	3.1×10^{-4}	2022	5
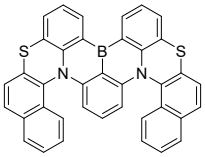 helicene-BN	2.1×10^{-3}	98%	2.0×10^{-3}	2022	6
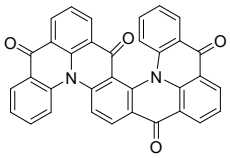 Hel-DiDikta	4.0×10^{-4}	4.1%	1.6×10^{-5}	2022	7

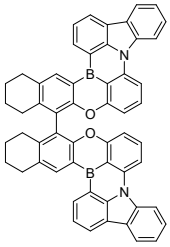 DOBN	1.0×10^{-3}	91%	9.1×10^{-4}	2022	8
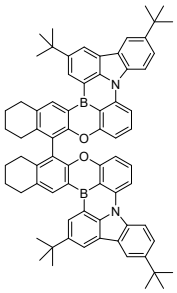 DOBNT	0.9×10^{-3}	96%	8.6×10^{-4}	2022	
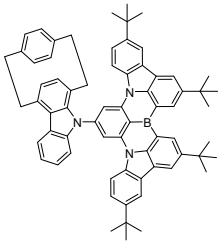 Czp-tBuCzB	0.54×10^{-3}	98%	5.3×10^{-4}	2023	9
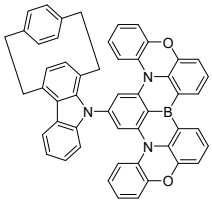 Czp-POAB	0.48×10^{-3}	93%	4.5×10^{-4}	2023	

Notes and references

(1) Xu, Y.; Wang, Q.; Cai, X.; Li, C.; Wang, Y. Highly Efficient Electroluminescence from Narrowband Green Circularly Polarized Multiple Resonance Thermally Activated Delayed Fluorescence Enantiomers. *Adv. Mater.* **2021**, *33*, 2100652.

(2) Wu, X.; Huang, J.-W.; Su, B.-K.; Wang, S.; Yuan, L.; Zheng, W.-Q.; Zhang, H.; Zheng, Y.-X.; Zhu, W.; Chou, P.-T. Fabrication of Circularly Polarized MR-TADF Emitters with Asymmetrical Peripheral-Lock Enhancing Helical B/N-Doped Nanographenes. *Adv. Mater.* **2022**, *34*, 2105080.

(3) Li, J.-K.; Chen, X.-Y.; Guo, Y.-L.; Wang, X.-C.; Sue, A. C. H.; Cao, X.-Y.; Wang, X.-Y. B,N-Embedded Double Hetero[7]helicenes with Strong Chiroptical Responses in the Visible Light Region. *J. Am. Chem. Soc.* **2021**, *143*, 17958-17963.

(4) Yang, S.-Y.; Zou, S.-N.; Kong, F.-C.; Liao, X.-J.; Qu, Y.-K.; Feng, Z.-Q.; Zheng, Y.-X.; Jiang, Z.-Q.; Liao, L.-S. A narrowband blue circularly polarized thermally activated delayed fluorescence emitter with a hetero-helicene structure. *Chem. Commun.* **2021**, *57*, 11041-11044.

(5) Yang, Y.; Li, N.; Miao, J.; Cao, X.; Ying, A.; Pan, K.; Lv, X.; Ni, F.; Huang, Z.; Gong, S.; et al.

Chiral Multi-Resonance TADF Emitters Exhibiting Narrowband Circularly Polarized Electroluminescence with an EQE of 37.2 %. *Angew. Chem., Int. Ed.* **2022**, *61*, e202202227.
(6) Yang, W.; Li, N.; Miao, J.; Zhan, L.; Gong, S.; Huang, Z.; Yang, C. Simple Double Hetero[5]helicenes Realize Highly Efficient and Narrowband Circularly Polarized Organic Light-Emitting Diodes. *CCS Chemistry.* **2022**, *4*, 3463-3471.
(7) dos Santos, J. M.; Sun, D.; Moreno-Naranjo, J. M.; Hall, D.; Zinna, F.; Ryan, S. T. J.; Shi, W.; Matulaitis, T.; Cordes, D. B.; Slawin, A. M. Z.; et al. An S-shaped double helicene showing both multi-resonance thermally activated delayed fluorescence and circularly polarized luminescence. *J. Mater. Chem. C.* **2022**, *10*, 4861-4870.
(8) Yan, Z.-P.; Yuan, L.; Zhang, Y.; Mao, M.-X.; Liao, X.-J.; Ni, H.-X.; Wang, Z.-H.; An, Z.; Zheng, Y.-X.; Zuo, J.-L. A Chiral Dual-Core Organoboron Structure Realizes Dual-Channel Enhanced Ultrapure Blue Emission and Highly Efficient Circularly Polarized Electroluminescence. *Adv. Mater.* **2022**, *34*, 2204253.
(9) Liao, X.-J.; Pu, D.; Yuan, L.; Tong, J.; Xing, S.; Tu, Z.-L.; Zuo, J.-L.; Zheng, W.-H.; Zheng, Y.-X. Planar Chiral Multiple Resonance Thermally Activated Delayed Fluorescence Materials for Efficient Circularly Polarized Electroluminescence. *Angew. Chem., Int. Ed.* **2023**, *62*, e202217045.